Electronic Supplementary Material (ESI) for Energy & Environmental Science.

Electronic Supplementary Information (ESI) for

Boosting water oxidation on metal-free carbon nanotubes *via* directional interfacial charge-transfer induced by adsorbed polyelectrolyte

Chunshao Mo,[§a] Junhua Jian,[§a] Jing Li,[a] Zhengsong Fang,[a] Zhe Zhao,[a] Zhongke Yuan,[a] Meijia Yang,[a] You Zhang,[a] Liming Dai,[*b] and Dingshan Yu[*a]

[a] Key Laboratory for Polymeric Composite and Functional Materials of Ministry of Education, School of Chemistry, Sun Yat-sen University, Guangzhou 510275, China

[b] Department of Macromolecular Science and Engineering, Case Western Reserve University, 10900 Euclid Avenue, Cleveland, OH 44106, USA

Experimental details

Chemicals and Materials.

All reagent and chemicals used were obtained from commercially sources. Poly(diallyl dimethylammonium) chloride (PDDA, average MW 200000-350000, 20 wt. % in H_2O), polyethylenimine (PEI, linear, average Mn 5000) and Nafion perfluorinated resin solution (5 wt. % in lower aliphatic alcohols and water, contain 15-20 % water) were purchased from Sigma-Aldrich Co. multiwall carbon nanotubes (MWCNTs, diameter: 20-40 nm) were purchased from Shenzhen Nanotech Port. Ltd. All chemicals and solvents were used without further purification unless otherwise stated.

Preparation of Free-standing PDDA@CNTs Composite Membranes.

Prior to use, the as-received commercial MWCNTs were thoroughly purified to remove the residual metal impurities by refluxing in 6 M hydrochloric acid instead of concentrated nitric or sulfuric acid, which avoided any oxidative treatment and the introduction of surface oxygen groups on the nanotubes.[1, 2, 3] Purified CNTs were collected by repeated centrifugation and washing with deionized water. Free-standing PDDA@CNTs composite membranes were produced by the vacuum filtration method. First, a predetermined amount of polyelectrolyte was dissolved in deionized water by stirring for 30 min with a magnetic stirrer (IKA Color Squid). Thereafter, a certain amount of pure CNTs was dispersed in the polyelectrolyte solution under sonication using a high frequency, low power sonic bath (Elmasonics, 40 kHz) with an aim to reduce the sonication effect on the polyelectrolyte and nanotubes. After sonicating for 20 min, the resulting homogeneous PDDA@CNT dispersion was vacuum-filtrated using a porous polyvinylidene fluoride (PVDF) filter membrane (Aisiwei, 0.8 μm pore size, 50 mm in diameter), forming a mat on the PVDF membrane. Finally, the mat attached PVDF membrane was vacuum-dried at 60 °C and subsequently subjected to mechanically peeling, eventually producing self-supported PDDA@CNTs composite membrane. By varying the mass ratios of the polymer to CNTs (10: 90 or 7: 93 or 5: 95), determined by thermogravimetric analysis (TGA) (Fig. S3), a series of PDDA@CNTs were obtained, which were denoted as PDDA@CNTs90, PDDA@CNTs93 and PDDA@CNTs95. Furthermore, reference membranes from the pristine CNTs, purified CNTs and PEI@CNTs, respectively, were prepared by following similar protocols.

Characterization.

Field-emission scanning electron microscopy (FE-SEM) images were recorded on a Hitachi S4800 SEM instrument at an acceleration voltage of 5.0 kV. Transmission electron microscopy (TEM) and high-resolution TEM (HRTEM) images were taken on a JEM-2010 HR field-emission electron microscope at an acceleration voltage of 200 kV. Thermogravimetric analysis (TGA) was carried out on a TG209F1 thermal analyzer at a heating rate of 10 °C min^{-1} in N_2. X-ray photoelectron spectroscopy (XPS) measurements were performed on an ESCA LAB250 X-ray photoelectron spectrometer. All XPS spectra were corrected using the C1s line at 284.0 eV, along with curve fitting and background subtraction. The inductively coupled plasma mass spectrometry (ICP-MS) characterization was done on a Thermo Fisher Scientific iCAP Qc Quadrupole instrument. Water contact angles (θ) were measured by using a drop shape analysis system (Kruss DSA100, Germany) at ambient temperature. Raman spectra were detected on a Renishaw micro-Raman system at an excitation wavelength of 514.5 nm.

KPFM Measurements.[4]

Kelvin probe force microscopy (KPFM) was carried out on a Bruker multimode 8 atomic force microscope (AFM) with the cantilever in a tapping mode. As a quantitative technology, KPFM can be used for evaluating changes of work function on the surface. The electrostatic force (F_e) between the tip and the sample can be described by the following equation:

$$F_e(z) = -\frac{dC}{dz}\Delta V^2 \qquad (1)$$

where z is the distance and C is the capacitance between the tip and sample. Provided with an AC voltage ($V_{ac}\sin\omega t$) and a DC voltage (V_{dc}) to a conductive tip, the voltage difference (ΔV) becomes $V_{dc} + V_{ac}\sin\omega t - V_{cpd}$. The equation can be divided into terms of frequency:

$$F_{dc}(z) = -\frac{1}{2}\frac{dC}{dz}\left(V_{dc} - V_{cpd}\right)^2 \qquad (2)$$

$$F_{1\omega}(z) = -\frac{1}{2}\frac{dC}{dz}\left(V_{dc} - V_{cpd}\right)V_{ac}\sin\omega t \qquad (3)$$

$$F_{2\omega}(z) = \frac{1}{4}\frac{dC}{dz}(\cos 2\omega t - 1)V_{ac}^2 \qquad (4)$$

Therefore, once the $1\,\omega$ signal is extracted from the AFM oscillation signal using the lock-in technique and a feedback system is applied to provide a signal to nullify the value, V_{cpd} can be obtained.

Electrode Preparation and Electrochemical Measurements.

As-synthesized free-standing membranes were transferred onto the polished glassy-carbon electrode (GCE) surface using Nafion (1 µL, wt 5 %) as the binder for WOR testing. Alternatively, the obtained membranes were also directly used as working electrodes for WOR without employing extra substrates or binders. All electrochemical measurements were performed on CHI 760E instrument (Shanghai, China) with a standard three-electrode configuration at room temperature with a Pt foil counter electrode and an Ag/AgCl (saturated KCl solution) reference electrode. Cyclic voltammograms (CVs) were recorded at a scan rate of 50 mV/s. Linear sweep voltammetric (LSV) curves were conducted at a scan rate of 10 mV/s with 90% IR-compensated unless specifically indicated. All of the LSV curves were recorded after applying a number of CV sweeps until they remained stable. Chronoamperometric curves were conducted at a constant potential without IR-compensated. The rotating ring-disk electrode (RRDE) with GC disk (0.247 cm^{-2}) and Pt ring (0.186 cm^{-2}) at a scan rate of 10 mV s^{-1} were performed at a rotating rate of 1600 rpm in N$_2$-saturated KOH solution. All potentials reported in this work were calibrated manually against the reversible hydrogen electrode (RHE) according to the following equation:

$$E_{\mathrm{RHE}} = E_{\mathrm{Ag/AgCl}} + 0.204\ \mathrm{V} + 0.0592\ \mathrm{V} \times \mathrm{pH} \qquad (5)$$

Where E_{RHE} is the potential calibrated against the RHE and $E_{\mathrm{Ag/AgCl}}$ is the potential obtained against the Ag/AgCl (saturated KCl solution) reference electrode, unless otherwise stated.

Calibration of the Reference Electrode.

The reference electrode (saturated Ag/AgCl) in our case was calibrated with respect to reversible hydrogen electrode (RHE) in hydrogen saturated 0.1 M KOH electrolyte.[5] In detail, LSV curve was recorded in a three-electrode cell using Pt foil as the working electrode, another Pt plate as the counter electrode, and saturated Ag/AgCl electrode as the reference electrode. Potentials were scanned from -1.1 to -0.8 V vs Ag/AgCl at various scan rates, as shown below

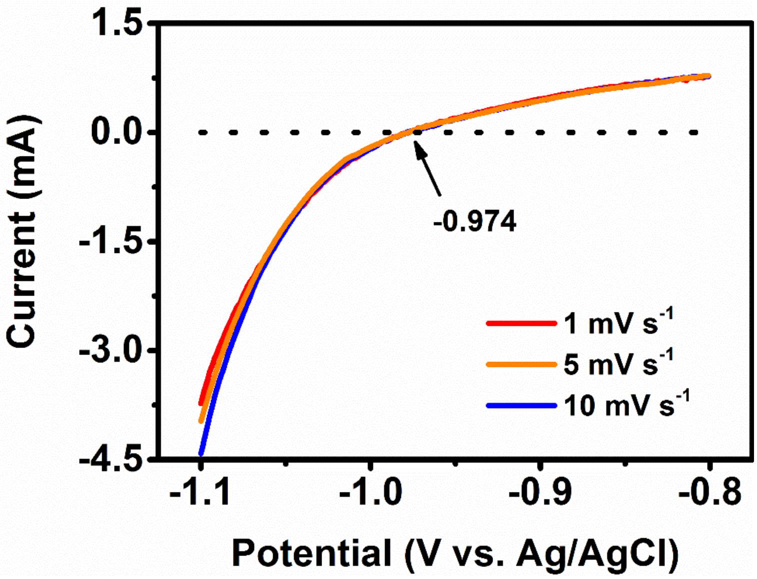

Fig. S1 LSV curves obtained with different scan rates in hydrogen (H_2)-saturated 0.1 M KOH solution.

The potential at which the current cross zero was considered as thermodynamic potential for the hydrogen electrode reaction, thus the potential vs RHE was calibrated. In our case, that is $E_{\mathrm{RHE}}= E_{\mathrm{Ag/AgCl}} + 0.974$, which was consistent with the equation 5: $E_{RHE} = E_{Ag/AgCl} + 0.204 + 0.059$ pH (pH = 13).

Density Functional Theory Calculations.

Density functional theory (DFT) calculations[6] were applied to calculate the absorption energy (E_a) of OH^- anion on the CNT surface with or without the polyelectrolyte, which can be defined by $E_a = E_{s+OH^-} - E_s - E_{OH^-}$, E_s, E_{OH^-} and E_{s+OH^-} are the energy of the adsorbing surface, OH^- anion and adsorbing surface $-OH^-$ compound. The DFT calculations were performed with Dmol3 package in Materials Studio of Accelrys Inc., in which the generalized gradient approximation (GGA) with the Perdew-Burke-Ernzerhof (PBE) exchange-correlation functional was employed. Also, an all-electron double numerical basic set with polarization functions (DNP) was used and the DFT-D correction (Grimme method) was applied to calculate the dispersion interactions. The solvation effect was considered by the COSMO model with water as the solvent. The convergence tolerances of energy, force, and displacement during geometry optimization were set to 1×10^{-5} Ha, 2.0×10^{-3} Ha/Å, and 5.0×10^{-3} Å, respectively. The surface of CNTs was simulated by periodically repeating monolayer graphene with a vacuum region of 40 Å, and the PDDA molecular chain was simplified to be small molecule derived from repeating units. In the case of PDDA wrapped CNTs the OH^- anion was placed between the CNTs surface and the simplified PDDA macromolecule.

Determination of Turnover Frequencies.

According to previously reported method.[7] The turnover frequency (TOF) for the water oxidation reaction could be calculated using following formula.

$$TOF\ (s^{-1}) = \frac{number\ \ of\ \ oxygen\ \ turnover\ \ /\ cm^2 geometric\ \ area}{active\ \ sites\ \ \ /\ cm^2 geometric\ \ area}$$

The number of oxygen turnover for WOR was calculated from the current density according to following equation.

$$\text{number of oxygen turnover} = \left(j\frac{mA}{cm^2}\right)\left(\frac{1\ \ Cs^{-1}}{1000\ \ mA}\right)\left(\frac{1\ \ mol\ \ e^-}{96485.3\ \ C}\right)\left(\frac{1\ \ mol\ \ O_2}{4\ \ mol\ \ e^-}\right) * 6.02 * 10^{23}$$

$$= \left(25.1\frac{mA}{cm^2}\right)\left(\frac{1\ \ Cs^{-1}}{1000\ \ mA}\right)\left(\frac{1\ \ mol\ \ e^-}{96485.3\ \ C}\right)\left(\frac{1\ \ mol\ \ O_2}{4\ \ mol\ \ e^-}\right) * 6.02 * 10^{23} = 3.92 * 10^{16}\ \ \left(\frac{s^{-1}}{cm^2}\right)$$

In our study, the positively charged carbon atoms on the side walls of CNTs are supposed to be active sites involved in the reaction. According to the atom configuration of CNT lattice, the possession area for each carbon atom on the side wall is calculated to be $0.144\ \ nm\ \ \times\ \ 0.864\ \ nm\ \ \times 0.5 = 6.22\ \ \times 10^{-2}\ \ nm^2$. So, the active site per real surface area and the value of TOF could be estimated.

$$active\ \ sites = \left(\frac{1\ \ atom}{6.22\ \ \times 10^{-2}\ \ nm^2}\right) = 1.61 * 10^{15}\ \ \left(\frac{sites}{cm^2}\right)$$

$$\text{TOF} = \frac{3.92 * 10^{16}\ \ \left(\frac{s^{-1}}{cm^2}\right)}{1.61 * 10^{15}\ \ \left(\frac{sites}{cm^2}\right) * A_{ECSA}} =\ \ 0.385\ \ s^{-1}$$

It should be noted that not all carbon sites were electrochemically accessible, thus the TOF was estimated to be a minimum value. Furthermore, our TOF value is comparable and even superior to many recently reported WOR catalysts (Please see Table S4).

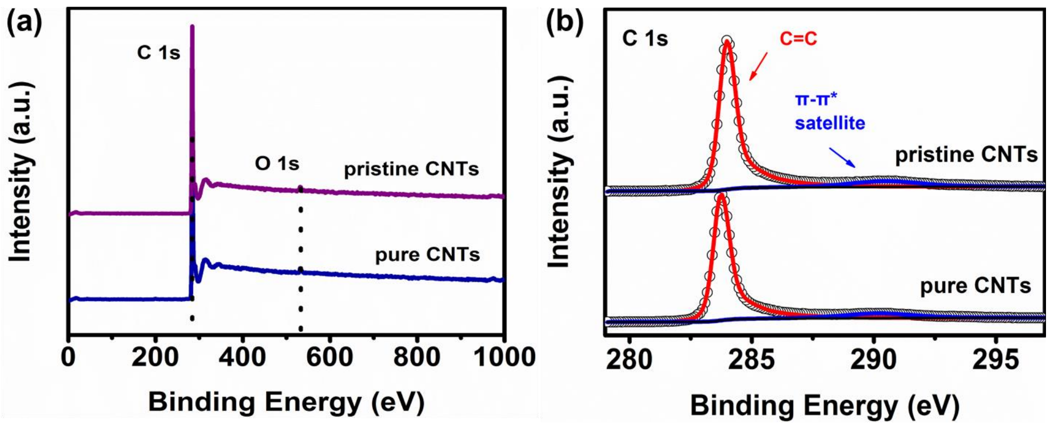

Fig. S2 (a) XPS survey of the pristine CNTs and pure CNTs. (b) High resolution XPS C 1s spectra obtained from the pristine CNTs and pure CNTs.

X-ray photoelectron spectroscopy was performed to verify the surface chemistry of CNTs after refluxing in hydrochloric acid. As shown in Fig. S2a, an asymmetric C1s peak was observed for both the pure CNTs and the pristine CNTs, while the trace amount of O (atomic ratio of O/C = 0.017) was possibly due to the existence of physically adsorbed oxygen since CNTs were susceptible to oxygen adsorption even at pressures as low as 10^{-8} to 10^{-10} Torr, during the XPS tests. [8-10] In our case, the XPS spectrum of the pristine CNTs shows a trace amount of oxygen (O/C = 0.017) and remained unchanged after purification. On the other hand, as shown in Fig. S2b, the high resolution C1s spectrum for the purified CNTs was almost the same as that of the pristine CNTs and highly ordered pyrolytic graphite (HOPG) and can be well fitted into only one C=C component at 284.0 eV without any oxygen-containing components at 286-289 eV. Moreover, no peak associated with heteroatom dopants (i.e. N at 398-402 eV, Cl at 200 eV) or metal impurities was observed in the XPS spectra for the CNTs after purification, indicating that no heteroatom was incorporated after the purification treatment and the metal residues, if any, have been largely removed. The above results clearly indicate that the nanotube structure was indeed free from oxygen groups, thus our purification process by HCl is indeed a non-destructed process, as demonstrated in previous studies.[11,12]

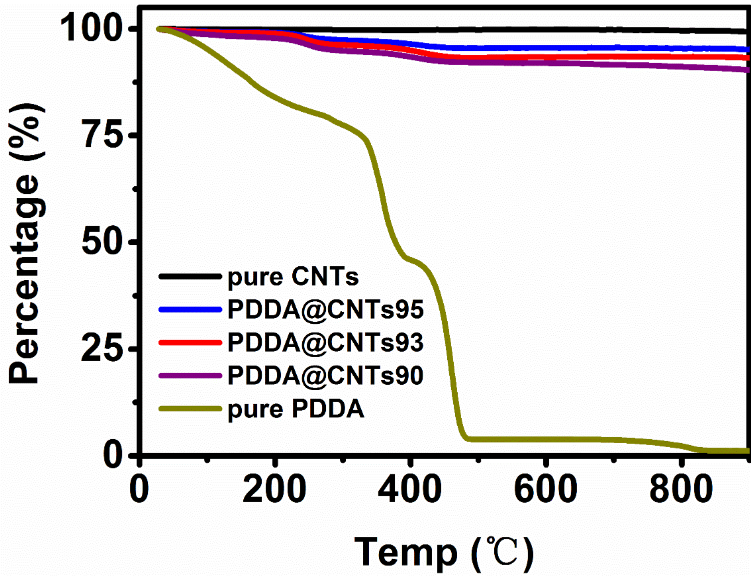

Fig. S3 TGA curves of the pure CNTs, pure PDDA, and various PDDA@CNTs samples with a heating rate of 10 ℃/min under nitrogen.

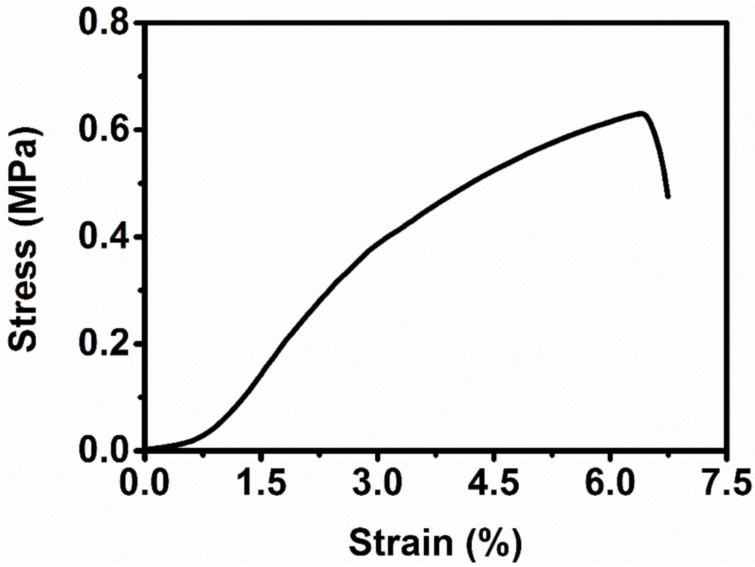

Fig. S4 The stress-strain curve of the PDDA@CNTs93 membrane.

The Young’s modulus for the PDDA@CNTs93 membrane was calculated to be 19.70 MPa.

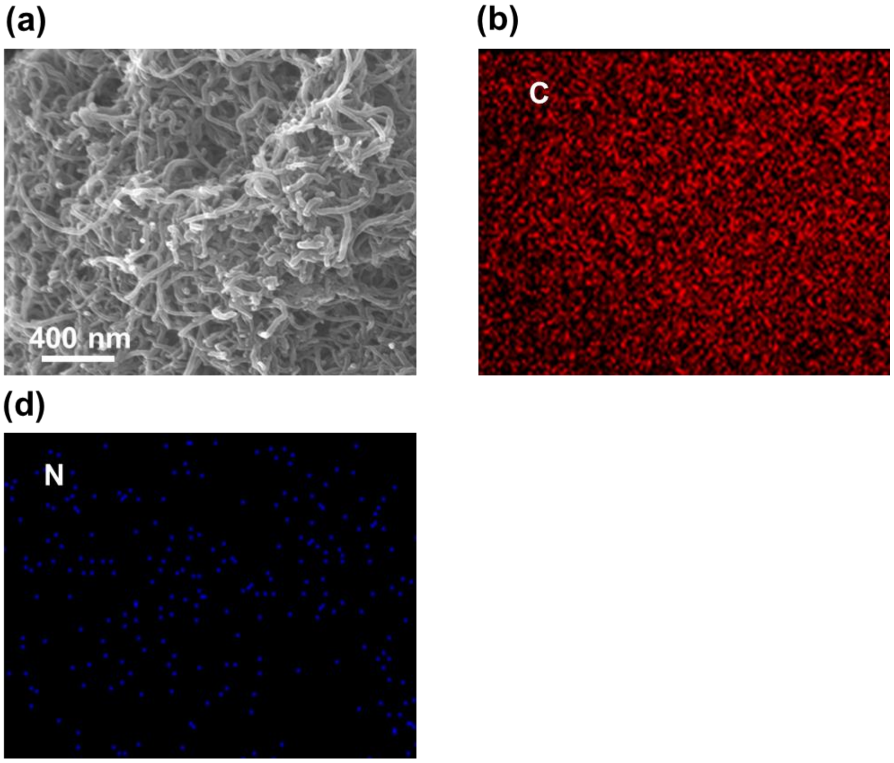

Fig. S5 Typical SEM image for the PDDA@CNTs93 membrane and the corresponding EDX elemental mapping for C and N.

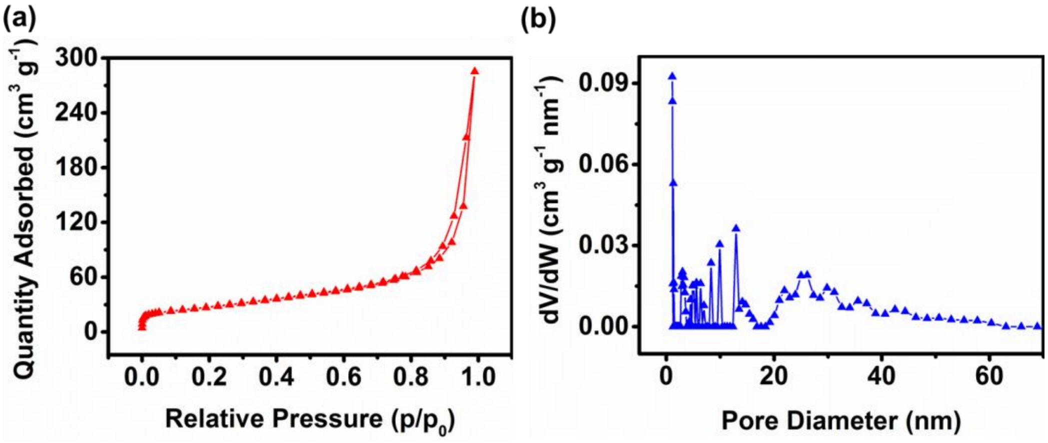

Fig. S6 (a) N_2 sorption isotherms of the PDDA@CNTs93 membrane and (b) pore size distribution.

The PDDA@CNTs93 membrane shows a mesoporous texture with a specific surface area of 97.5 m^2 g^{-1} and a total pore volume of 0.44 cm^3 g^{-1}.

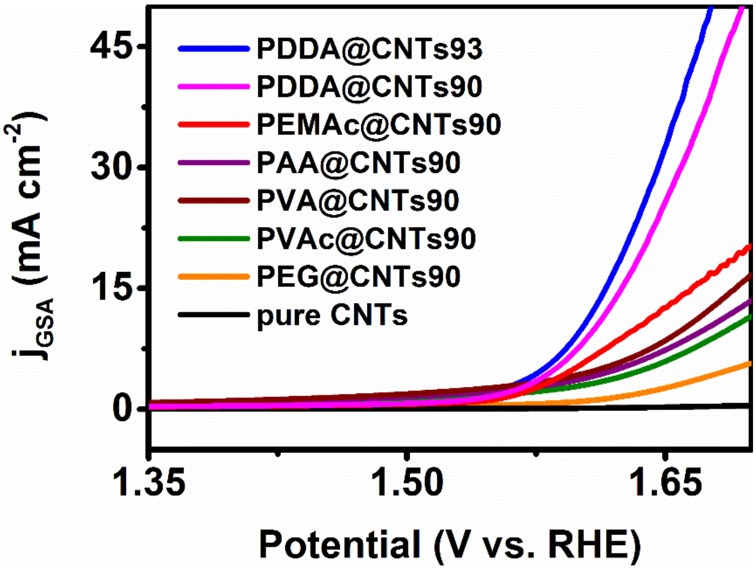

Fig. S7 LSV curves of various catalysts including PDDA@CNTs93, PDDA@CNTs90, PEMAc@CNTs90, PAA@CNTs90, PVA@CNTs90, PVAc@CNTs90, PEG@CNTs90 and pure CNTs in 0.1 M KOH solution (90% IR-compensated), the WOR current is normalized to the geometric area of electrodes. Note: as control experiments, PAA@CNTs90, PVA@CNTs90, PVAc@CNTs90 and PEG@CNTs90 were respectively produced according to our previous report. [1]

As can be seen in Fig. S7 and Table S3, the PDDA wrapped CNT catalysts (PDDA@CNTs93 and PDDA@CNTs90) in 0.1 M KOH present much better WOR activities with a lower overpotential compared with those CNT catalysts wrapped with polymers containing polar oxygen groups, including poly(ethylene-alt-maleic acid) (PEMAc), poly(vinyl alcohol) (PVA), poly(vinyl acetate) (PVAc), poly(ethylene glycol) (PEG)) (404-470 mV at 10 mA cm^{-2}).[1] This result indicates that our newly-developed PDDA wrapping strategy is indeed more effective to boost the WOR activity of CNTs especially in lower KOH concentration (0.1 M KOH) with respect to the previously-reported strategy using polymers with polar oxygen-containing groups.[1]

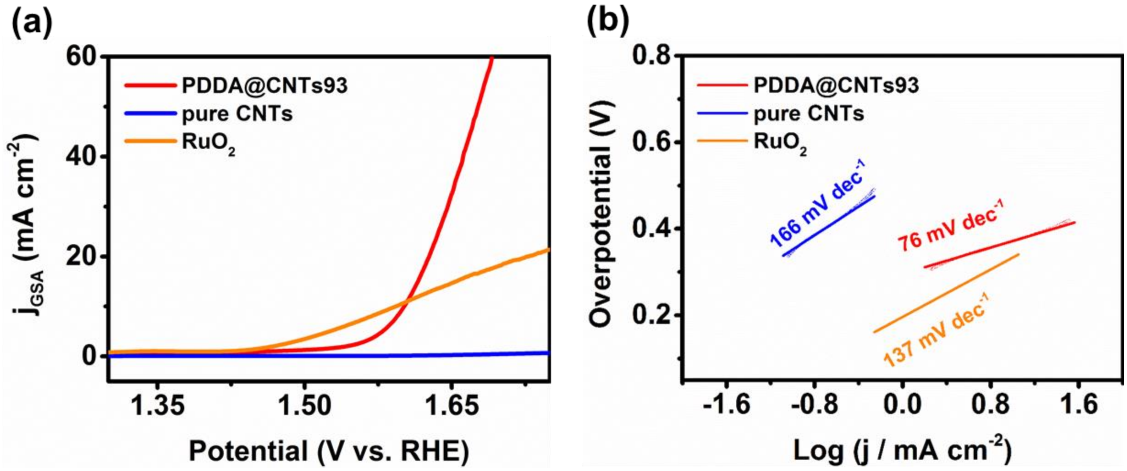

Fig. S8 (a) LSV curves of the PDDA@CNTs93, pure CNTs and RuO_2 in 0.1 M KOH (90% IR-compensated), (b) and the corresponding Tafel plots.

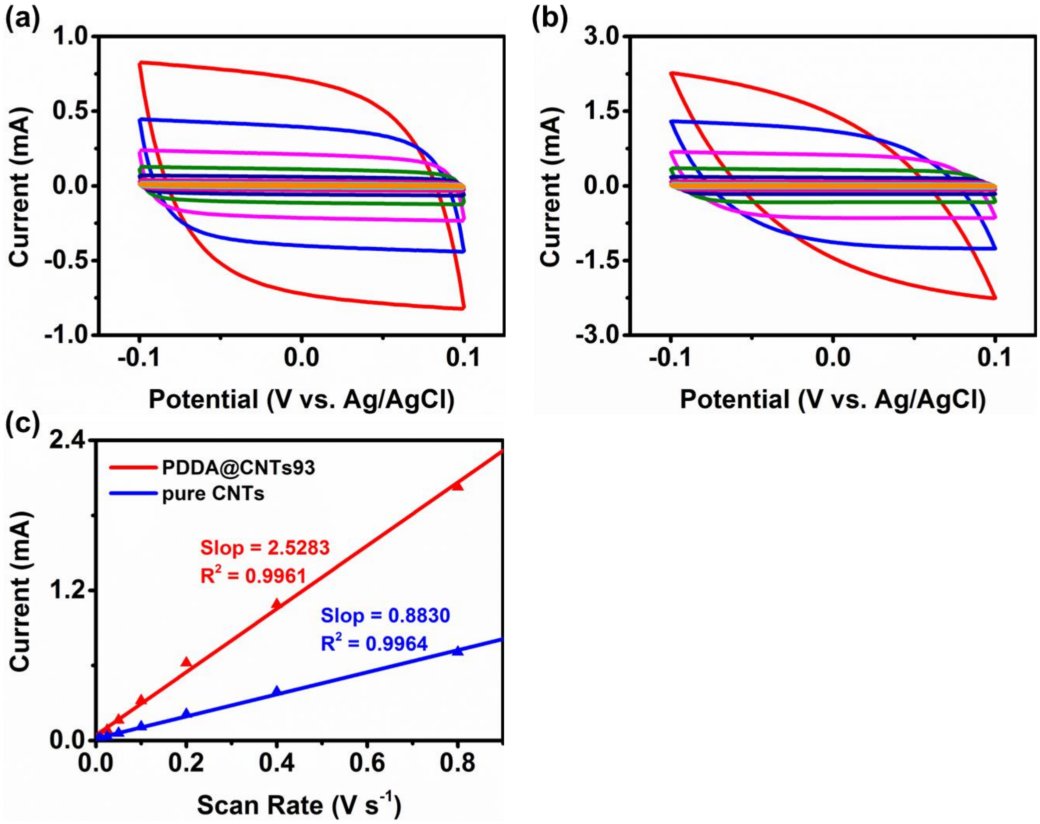

Fig. S9 Cyclic voltammograms obtained with (a) pure CNTs and (b) PDDA@CNTs93 loaded on glassy carbon electrodes (-0.1 V ~ 0.1 V vs. Ag/AgCl) at scan rates of 5, 10, 25, 50, 100, 200, 400, 800 mV s^{-1} in 0.1 M KOH solution, respectively. (c) The anodic capacitance currents plotted as a function of scan rate. The double-layer capacitance determined from this system is taken from the average of the absolute value of anodic slopes of the linear fits.

The electrochemical active surface area (ECSA) for different catalysts were derived from the electrochemical double-layer capacitance (C_{DL}) by measuring the non-Faradaic capacitive current with scan-rate dependence of cyclic voltammograms (CVs).[13, 14] To determine double-layer capacitance via CV, a potential range in which no apparent Faradaic processes occur was applied for CV in 0.1 M KOH solution and the charging current (i_c) was recorded at multiple scan rates (v). Briefly, the double layer capacitance (C_{DL}) was given in equation 1.

$$i_c = v\ \mathrm{C_{DL}} \tag{1}$$

Therefore, a plot of i_c as a function of v gives a straight line with a slope equal to C_{DL} and the C_{DL} of PDDA@CNTs93 and pure CNTs were measured to be 2.5283 mF and 0.8830 mF, respectively. The ECSA calculation of the catalysts was based on equation 2.

$$\mathrm{ECSA} = \frac{\mathrm{C_{DL}}}{\mathrm{C_S}} \tag{2}$$

where C_S is the specific capacitance of carbon C_S=0.040 mF cm^{-2} adopted from previous reports.[8] As a result, the ECSA of the PDDA@CNTs93 and pure CNTs was calculated to be 63.2 cm^{-2} and 22.3 cm^{-2}. There is no surprise to see that the ECSA for CNTs increased after polymer wrapped due to facilitating C_{DL} and improved electrolyte wettability, in accordance to the previous publications. [15-18]

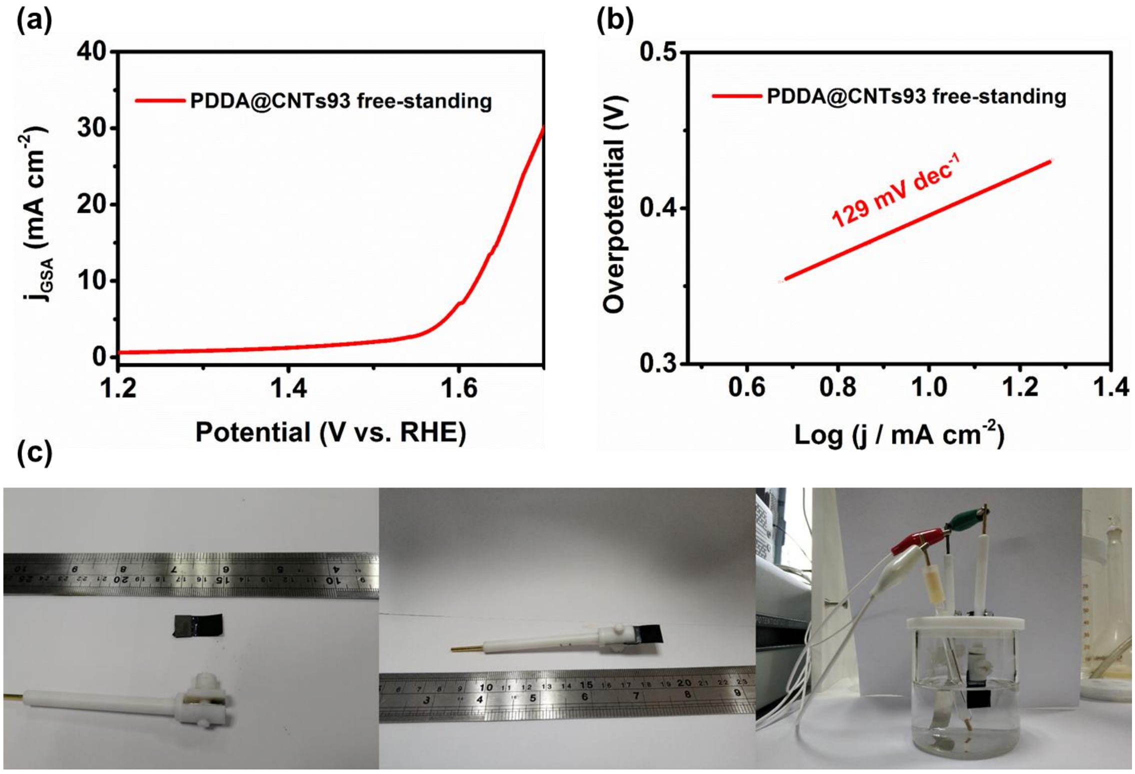

Fig. S10 (a) LSV curves of PDDA@CNTs93 free-standing membrane directly used as the electrode in 0.1 M KOH solution and (b) the corresponding Tafel plot. (c) The digital photos for WOR testing of PDDA@CNTs93 free-standing membrane: Briefly, a platinum-based electrode holder was applied to fix the film sample by forming a sandwich structure. Furthermore, the commercially available Super glue was used for region-specific masking to ensure the area of the catalyst membrane immersed in the electrolyte was 1 cm × 1 cm. It is worth to note that only the catalyst membrane was immersed in the electrolyte during electrochemical test.

As can be seen in Fig. S10, the free-standing PDDA@CNTs93 membrane electrode exhibited good WOR performance with a low overpotential of 390 mV at 10 mA cm^{-2} and a low Tafel slope of 129 mV dec^{-1} in 0.1 M KOH. Notably, the PDDA@CNTs93 membrane catalyst used directly as the working electrode exhibited a slightly increased overpotential relative to the counterpart casted on rotating disk electrode (RDE). Such slight activity degradation was mainly caused by the relatively poor mass transport and the blockage effect of evolved oxygen bubbles on the catalyst surface under testing condition without rotation. As demonstrated in previous reports,[19] the gas bubbles coalescence occurred frequently on the oxygen evolving electrode, and the adherent oxygen bubbles on the electrode could hinder the electrolyte access to the active sites, leading to a fractional blockage of the active sites. Thus, most WOR catalysts were casted onto the RDE electrode and then tested with the rotation. With the help of rotation and fast electrolyte flow, the accumulation of evolved oxygen bubbles on RDE could be largely avoided and the adherent bubbles could be removed quickly.[19] Meanwhile, the rotation also facilitated rapid mass transport. In a sharp contrast, when the membrane catalyst was directly used as the working electrode, there was no any rotation involved during WOR testing. Thus, due to the blockage effect of adherent gas bubble on the active sites and relatively poor mass transport, the membrane catalyst showed slight degradation relative to its counterpart deposited on RDE.

Fig. S11 Photograph of PDDA@CNTs93 loaded rotating disk electrode when the applied potential is above the onset potential of WOR (1.47 V), showing O_2-bubbles on the electrode surface.

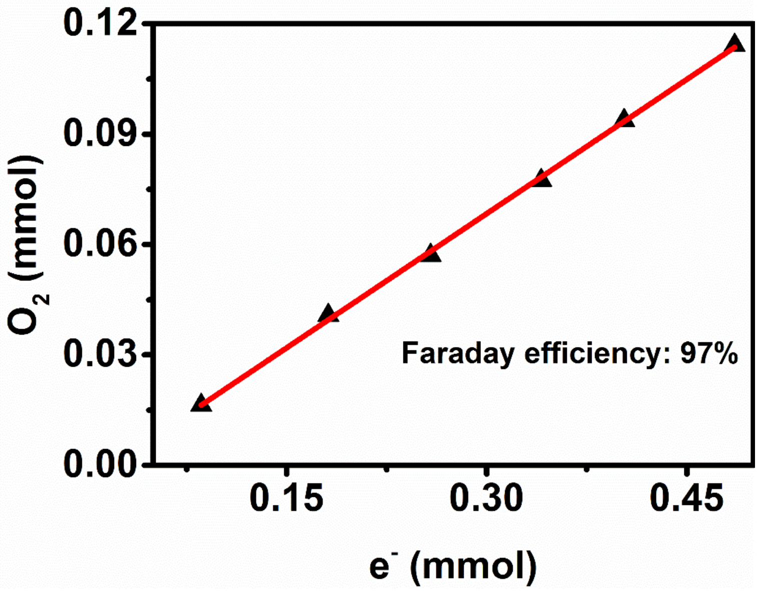

Fig. S12 Comparison of evolved O_2 vs. the amount of consumed e^{-1} during the course of electrolysis.

Faraday efficiency was determined from volumetric method.[20] The oxygen gas generated on the catalyst casted glassy-carbon electrode was carefully collected in a 10 mL graduated tube, which was filled with the electrolyte. Galvanostatic electrolysis was applied to the work electrode with a current density of 5 mA cm^{-2} for about 6 h under ambient conditions (25 ºC, 1 atm). The evolved oxygen gas volume was recorded at every 4000 s and the total charges passing through working electrode were calculated by current × time. Gas chromatograph (Shimadzu GC-2014) was further employed to evaluate the purity of generated gaseous product, and only O_2 was detected throughout the test without any other impurities.

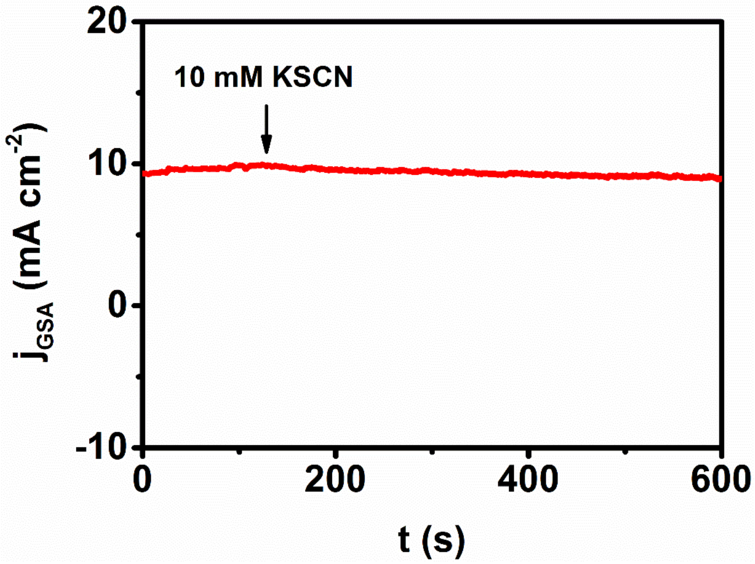

Fig. S13 Chronoamperometric response of PDDA@CNTs93 in 0.1 M KOH solution with the addition of KSCN (resulting in an electrolyte with 10 mM KSCN).

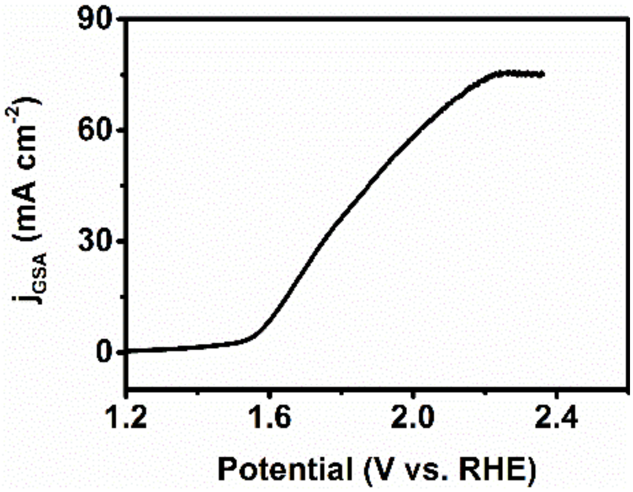

Fig. S14 LSV curve of PDDA@CNTs93 in a wide potential window of 1.2-2.4 V vs. RHE in 0.1 M KOH. (without IR-compensated)

As shown in Fig. S14, the current density for PDDA@CNTs93 showed a steady increase until the scanning potential reaches 2.2 V vs. RHE in relatively low KOH concentration (0.1 M). However, above 2.2 V vs. RHE, the current density leveled off, which could be ascribed to severe corrosion of catalysts or destruction of electrode structures.

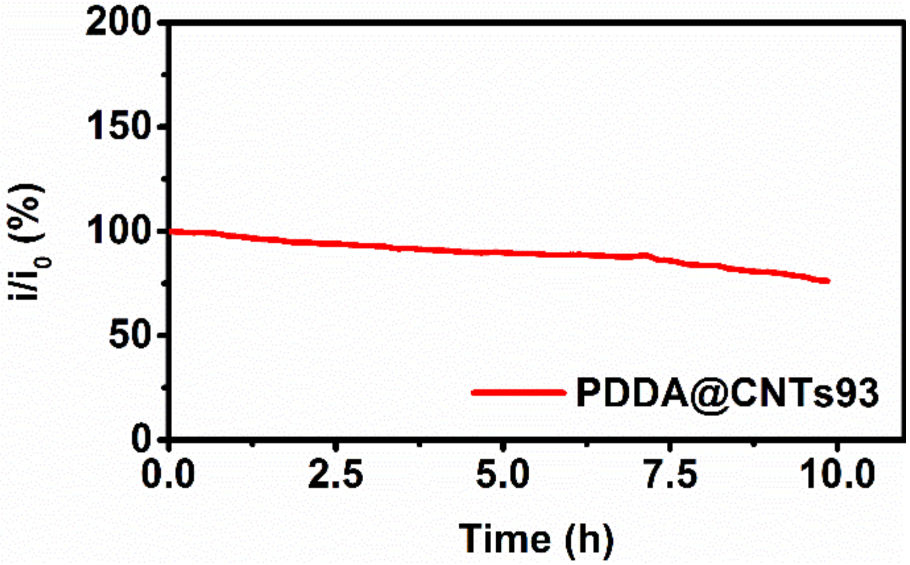

Fig. S15 Chronoamperometric curve for PDDA@CNTs93 obtained at constant current density (j=3.5 mA cm^{-2}) after 10 hrs.

As can be seen in Fig. S15, the catalytic current retention is still as high as 77 % over 10 hrs, which is comparable and even superior to some recently reported WOR catalysts,[21a-c] indicating a good operation stability for our catalysts. The current loss should be mainly from possible partial release of PDDA into the electrolyte. Nevertheless, previous studies have proved that some water-soluble polymer, such as PEI, can irreversibly adsorb onto the sidewalls of the CNTs, and the adsorbed polymer chains with multiple anchoring points cannot be readily removed from the nanotubes even by extensively rinsing with good solvents.[21d] Thus, it is not surprised that our polymer wrapped CNT catalysts have a good long-term stability. Similarly, previously reported CO_2 reduction catalysts based on water soluble polymer coated CNT materials[21e] were also demonstrated to show good long term stability.

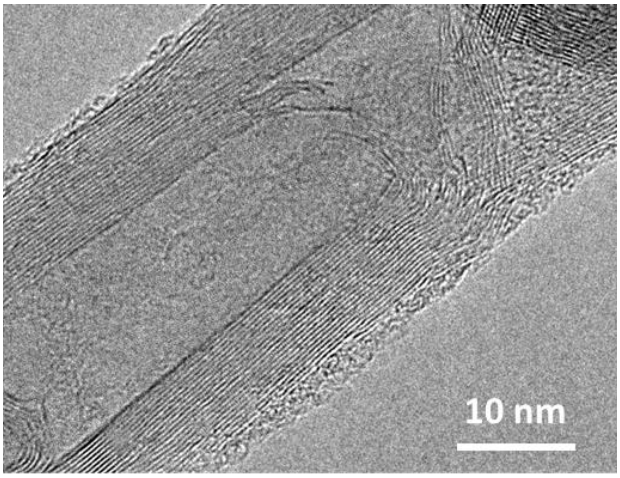

Fig. S16 TEM images of PDDA@CNTs93 after long-term chronoamperometric testing.

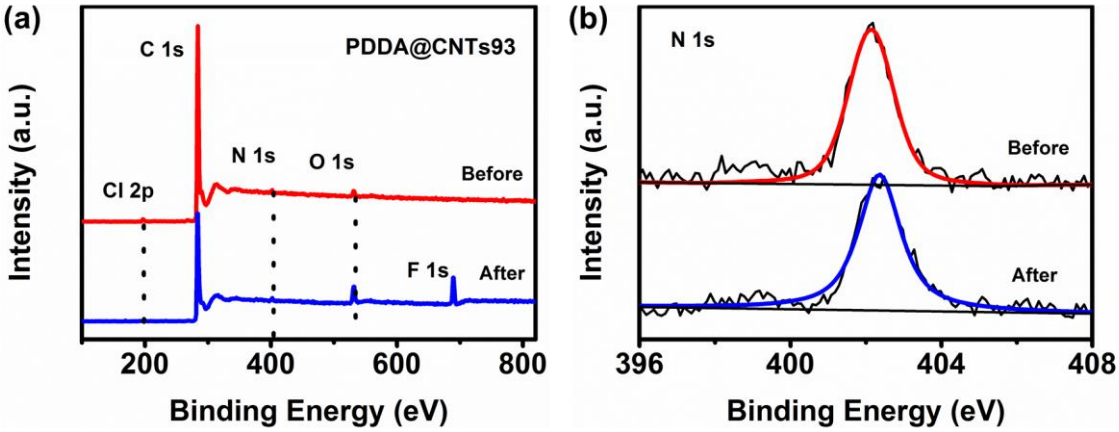

Fig. S17 (a) XPS survey spectra and (b) high resolution XPS N1s spectra of PDDA@CNTs93 before and after long-term chronoamperometric testing comparison.

After long-term i-t electrochemical testing, thin PDDA adlayer attaching to the outer wall of CNTs could be observed in HRTEM image. Also, the XPS spectrum of PDDA@CNTs93 gives an N1s peak at similar position after long-term chronoamperometric testing further confirmed the excellent stability of the composite catalysts. The present of F1s peak comes from the Nafion used during the electrode preparation.

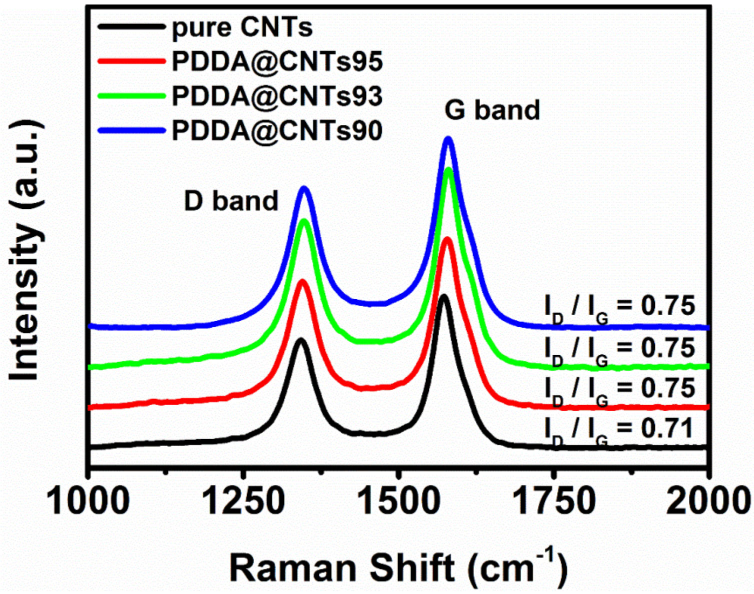

Fig. S18 Raman spectra of pure CNTs and various PDDA@CNTs sample.

Raman spectra for pure CNTs and various PDDA@CNTs shown in Fig. S18 reveal similar D and G bands centered at ~1350 cm^{-1} and ~1580 cm^{-1} respectively. However, the G band of CNTs revealed significant upshift, indicating strong charge-transfer interaction between CNTs and PDDA, since the presence of such interaction can be manifested by the shift of the G band position, as demonstrated in previous reports.[10, 22] Notably, the slight increase of the intensity ratio of the D/G band (I_D/I_G) was also observed for PDDA@CNTs, implying the effective polymer coating on the nanotubes.[23]

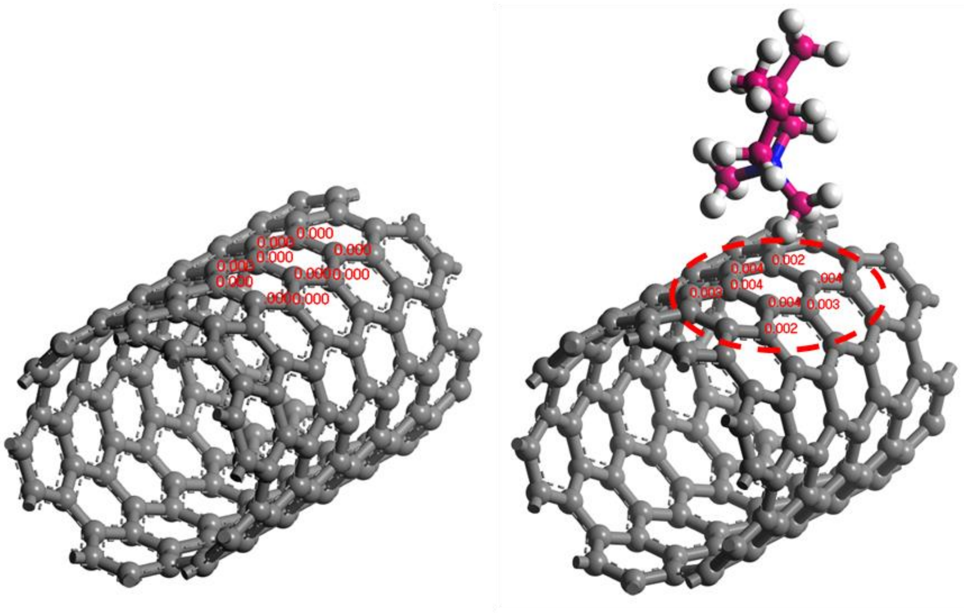

Fig. S19 Calculated charge density distribution for (a) a single carbon nanotube and (b) carbon nanotube attached with one constitutional repeating unit of PDDA.

The brief simulation was also performed with DMol3 in the Materials Studio (Accelrys Inc.) software with the same setting as DFT calculations in the main text.[24] Obviously, the carbon atoms nearby the PDDA unit exhibited positive charge density (0.002-0.004) compared with those on single nanotube (0.000). This result renders theoretical support for our claim that “p-doping” by PDDA can create positively charged carbon sites on the CNTs via intermolecular charge transfer, which agreed with KPFM and Raman results. Notably, during the simulation, the PPDA polymer chain was simplified to be only one unit, thus several adjacent carbon atoms exhibited obvious change in charge density. In fact, the whole CNT surface was coated with a layer of PDDA. As such, if the whole polymer chain is chosen for simulation, it can be expected that high density of positively charge carbon sites can be generated on the nanotube side along the whole interface.

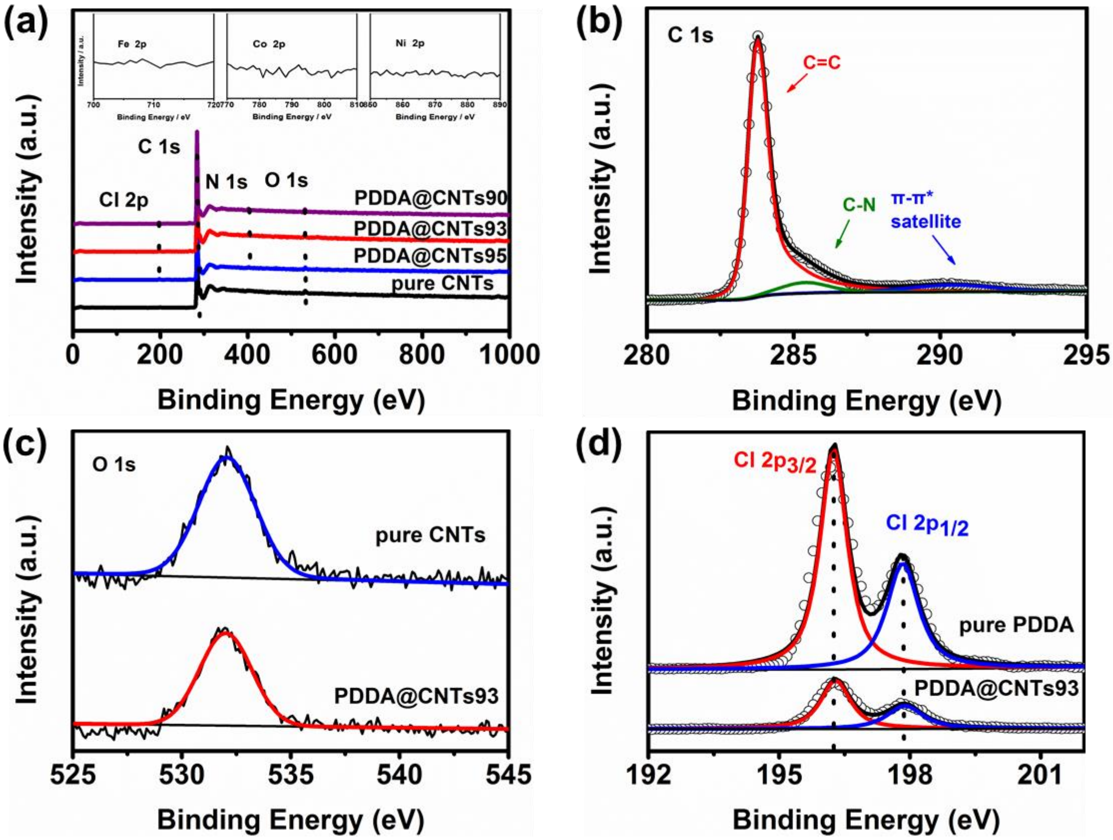

Fig. S20 (a) XPS survey spectra of the pure CNTs and various PDDA@CNTs. Insets are the high resolution of Fe2p, Co2p, Ni2p obtained from pure CNTs, respectively. (b) High resolution XPS C1s spectra obtained from PDDA@CNTs93. (c) High resolution XPS O1s spectra obtained from pure CNTs and PDDA@CNTs93. (d) High resolution XPS Cl2p spectra obtained from pure PDDA and PDDA@CNTs93.

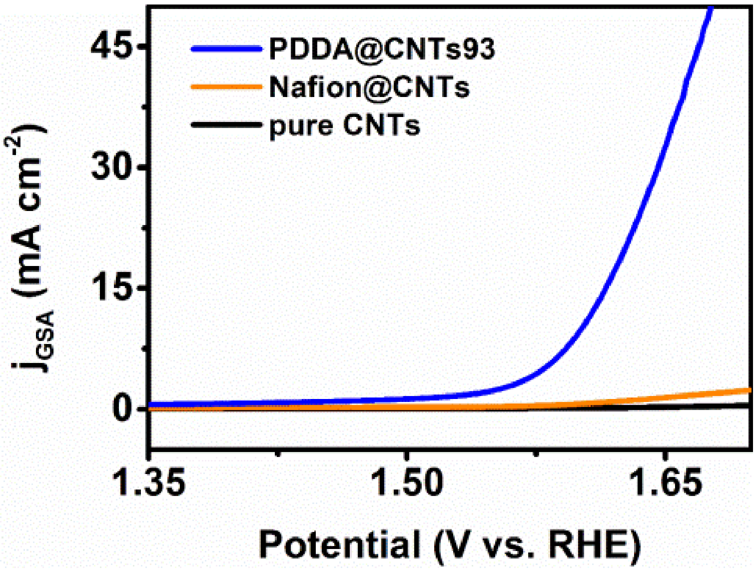

Fig. S21 LSV curves of PDDA@CNTs93, Nafion@CNTs93 and pure CNTs in 0.1 M KOH solution (90% IR-compensated). Note: as a control experiment, we prepared the Nafion@CNTs composite membranes following similar protocols as that of PDDA@CNTs93. Nafion solution was used as received and the weight content of Nafion in the composite membrane was similar to the case of PDDA.

As shown in Fig. S21, the WOR activity of Nafion@CNTs was much inferior to that of PDDA@CNTs and exhibited a negligible enhancement with respect to that of pure CNTs. This result rules out the effect of the Nafion binder. According to our previous report,[1] some polymers containing polar groups, such as -COOH, -OH, -$COOCH_3$, and -O-, can be used to modify CNTs to improve the WOR activity. The enhanced mechanism lies in that the oxygen groups from polymers are prone to interact with the H-carrying WOR intermediates (e.g., OH* and OOH*) through H-bonding interactions and regulate the adsorption of the WOR intermediates.[1] However, various polar oxygen groups afford different levels of hydrogen bonding interaction and thereby various regulation ability of adsorption energy of intermediates, eventually yielding various degrees of activity enhancement for various polymers.[1] Among polymers with various polar groups such as PEMAc, PAA, PVA, PVAc and PEG, the PEMAc@CNT catalyst exhibited the largest activity enhancement relative to pure CNTs, while PEG@CNT only showed slight activity enhancement (see Table S3). This indicates that not all polymers with polar chemical groups can greatly boost the WOR activity of CNTs, which depends on the nature of polar groups and the interaction strength between the polar groups and WOR intermediates. In the case of Nafion, unlike PDDA, Nafion has no charge-transfer ability and OH^- trapping capacity. The polar sulfonate groups in Nafion afforded only a weaker hydrogen bonding interaction with OH* and OOH*, thus, the Nafion@CNTs yielded a negligible activity enhancement relative to pure CNTs, in a sharp contrast to the PDDA@CNTs with remarkable activity enhancement. Therefore, the effect of Nafion on the OER performance can be largely ruled out despite it has polar chemical groups.

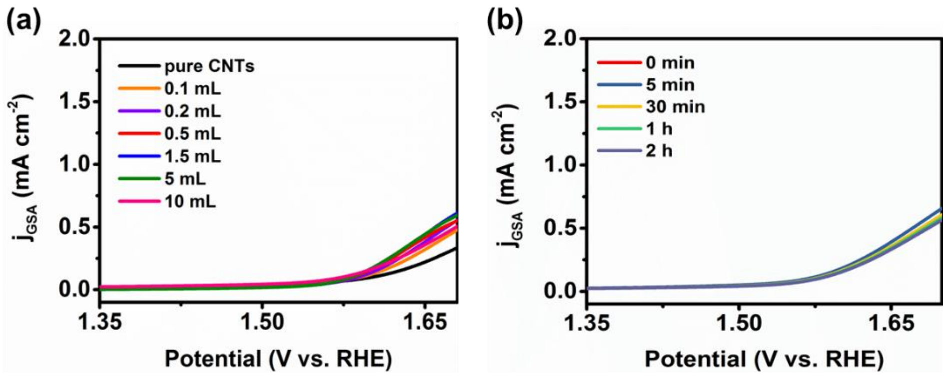

Fig. S22 (a) LSV curves of pure CNT membrane catalyst in 50 mL 0.1 M KOH solution with the addition of 0.1, 0.2, 0.5, 1.5, 5 and 10 mL poly(diallyl dimethylammonium) chloride (PDDA, average MW 200000-350000, 20 wt. % in H_2O) after stirring for 30 min. (b) LSV curves of pure CNT membrane catalyst in 50 mL KOH solution with the addition of 1.5 mL PDDA after stirring for 0 min, 5 min, 30 min, 1 h and 2 h. As can be seen, direct addition of PDDA into the KOH electrolyte could not readily boost the WOR performance of CNTs.

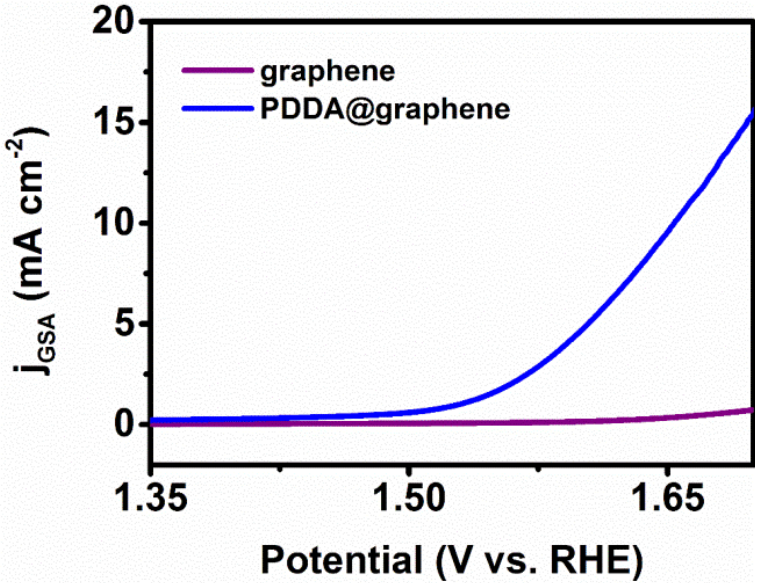

Fig. S23 LSV curves of PDDA@graphene and graphene in 0.1 M KOH solution (90% IR-compensated).

As a control experiment, exfoliated graphene was purchased from Nanjing XFNANO Materials Tech Co. and used as received. The PDDA@graphene catalyst was prepared by following the same protocol with that of PDDA@CNTs. The mass ratio of PDDA in the PDDA@graphene catalyst was similar to that of PDDA@CNTs93.

As can be seen in Fig. S23, the PDDA@graphene catalyst demonstrated much better WOR performance with a lower overpotential at 10 mA cm^{-2} and earlier onset potential relative to the pure graphene. This result indicates that our PDDA wrapping strategy is versatile and can be also applied to other carbon materials for boosting their WOR activities.

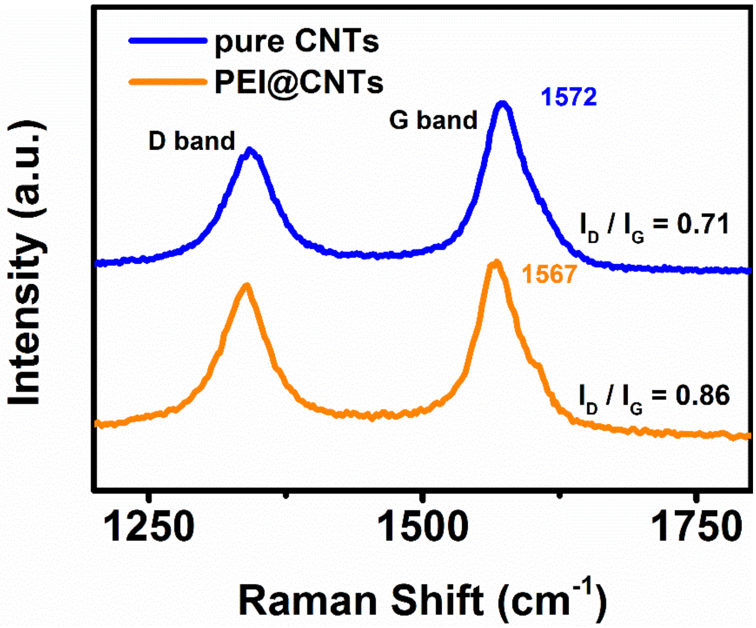

Fig. S24 Raman spectra of pure CNTs and PEI@CNTs.

Similar to the PDDA@CNTs, Raman spectra for PEI@CNTs also shows slight increase of the intensity ratio of the D/G band (I_D/I_G) but with significant downshift of G band, indicating the charge transfer from PEI to CNTs, denoted as “n-doping” of CNTs.

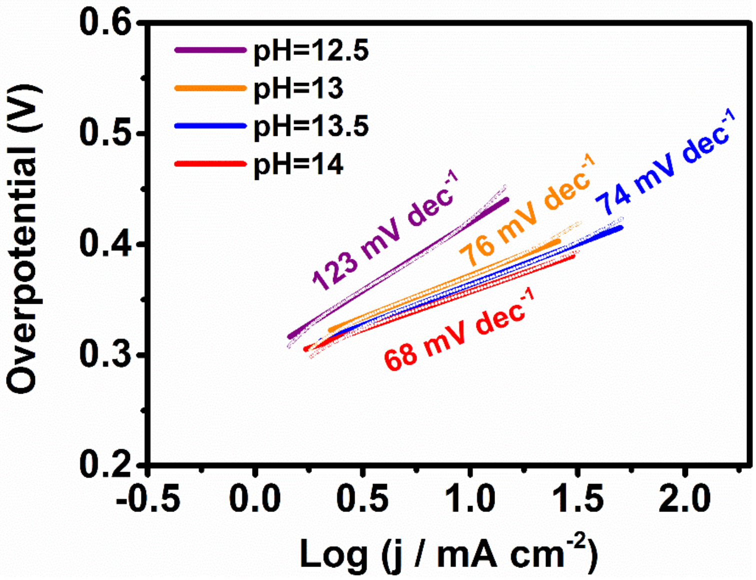

Fig. S25 The Tafel plots of PDDA@CNTs93 in KOH solution (pH=12.5, 13, 13.5, 14).

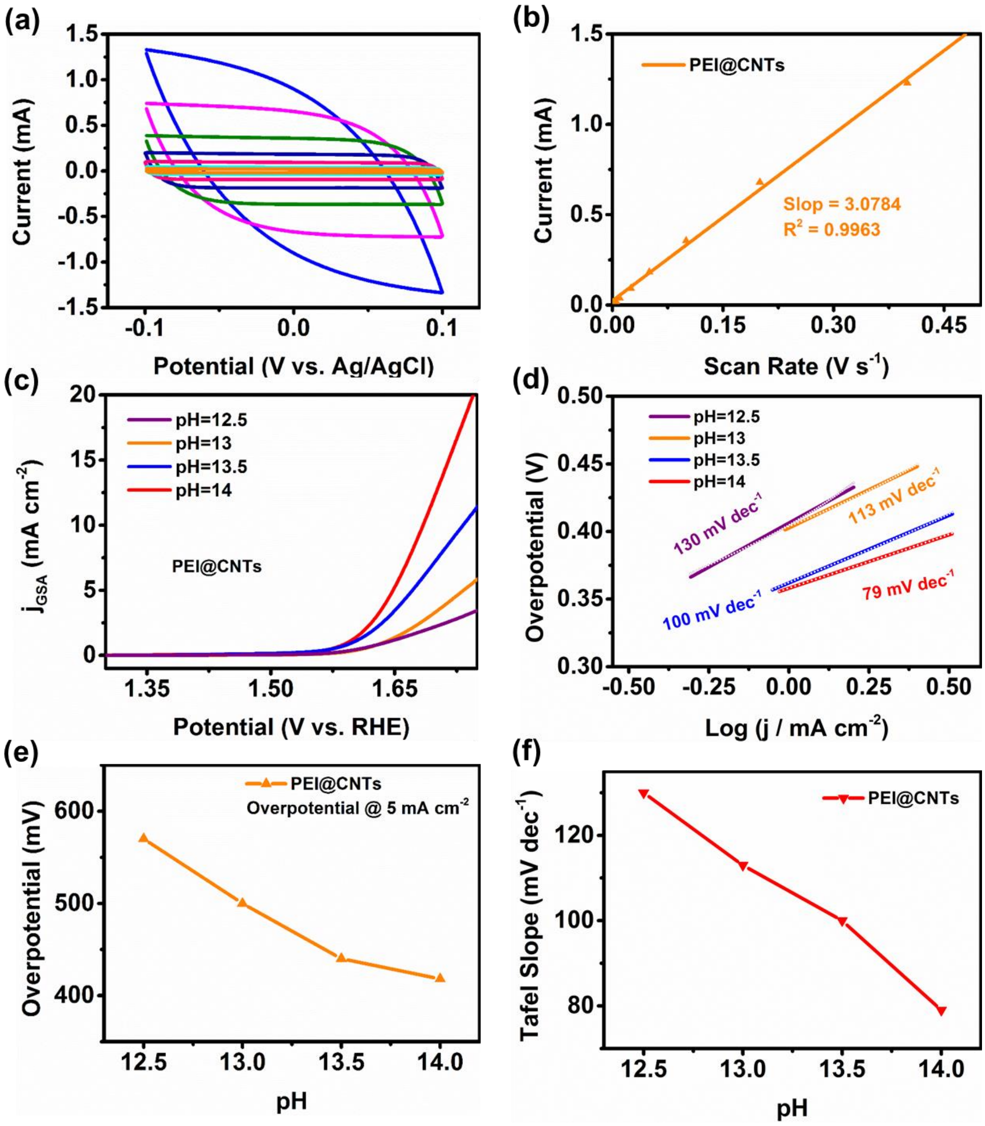

Fig. S26 (a) Cyclic voltammograms obtains with PEI@CNTs loaded on glassy carbon electrodes in the capacitance current range (-0.1 V ~ 0.1 V vs. Ag/AgCl) at a scan rates of 5, 10, 25, 50, 100, 200, 400 mV s^{-1} in 0.1 M KOH solution, respectively. (b) The anodic capacitance currents plotted as a function of scan rate. (c) LSV curves of PEI@CNTs as a function of pH (pH = 12.5, 13, 13.5, 14), (d) and corresponding Tafel plots. (e) Overpotential plots at 5 mA cm^{-2} and (f) Tafel plots of PEI@CNTs as a function of pH (pH =12.5, 13, 13.5, 14).

The electrochemical active surface area (ECSA) for PEI@CNTs membrane was calculated by following the same method with PDDA@CNTs93. As a result, the electrochemical double-layer capacitance (C_{DL}) was measured to be 3.0783 mF, and the corresponding ECSA was 77.0 cm^2.

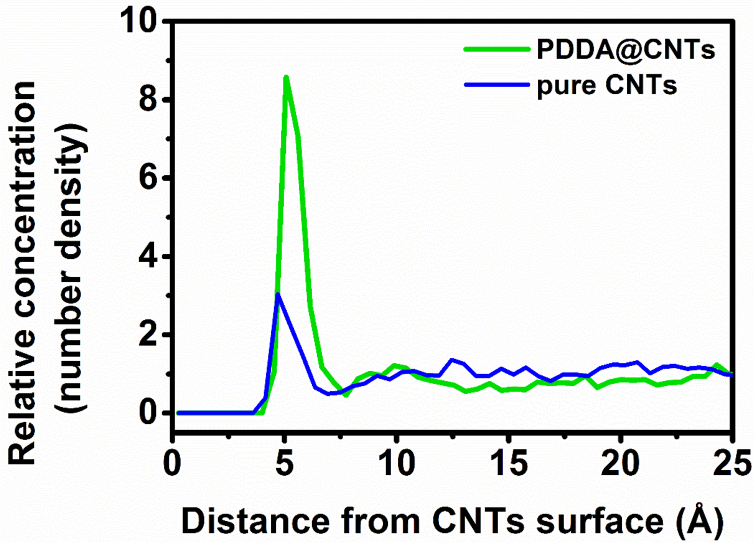

Fig. S27 Molecular dynamics simulation regarding relative number density of OH^- anion as a function of the distance from the CNTs surface in 1 M KOH.

To determine the influence of PDDA on the local OH^- concentration near the CNTs surface, a molecular dynamics (MD) calculation was carried out.[25] To begin with, the CNT surface was abstracted to be a graphene plane (25 Å ×25 Å) and PDDA was simplified to be molecular chain containing 5 repeating units. Further, the KOH solution with certain concentration (0.1 M or 1 M) was placed on the surface. Typically, water molecules were filled in the periodic cell to fabricate a water box with a density of 1.05 g cm^{-3} at 298 K. The amount of electrolyte ions was determined by the solution concentration (1 mol L^{-1} KOH solution denoted that K^+: OH^-: H_2O = 1: 1: 55).[20] Also, the charge neutrality of the whole system should be maintained. All MD simulations were performed and analyzed with Forcite package in Materials Studio of Accelrys Inc., and condensed phase optimized molecular potential (COMPASS) forcefield was employed. Here, the system configuration was optimized, followed by the MD simulations with carbon atoms frozen in positions. All structure optimization was carried out using smart algorithm with quality level set to ultrafine. MD simulation was performed at 298 K NVT ensemble with Berendsen thermostat for 2.5 ns to allow the systems indeed reach thermal equilibrium state and the last 1 ns was taken for the concentration profile analysis.[26] The electrolyte region was split into a set of bins (approximately 0.5 Å in width) along the perpendicular direction of carbon surface. The concentration (relative number densities) of OH^- was determined by calculating the ratio of volumetric number density in each bin over that in electrolyte bulk.

Table S1. Comparison of selected state-of-the-art metal-free WOR electrocatalysts in KOH solution (pH = 13).

Catalysts	**Overpotential at 10mA cm^{-2} (mV)**	**Tafel slope (mV dec^{-1})**	**Substrate**	**Electrolyte**	**References**
PDDA@CNT93	370	76	GCE	0.1 M KOH	This work
N-graphene/CNT	420	/	GCE	0.1 M KOH	Ref 27
g-C_3N_4/G	539	68.5	GCE	0.1 M KOH	Ref 28
OCC-8	477	82	CC	0.1 M KOH	Ref 29
N/C	380	/	GCE	0.1 M KOH	Ref 30
echo-MWCNTs	450	72	GCE	0.1 M KOH	Ref 13
NGSH	400	83	GCE	0.1 M KOH	Ref 31

Table S2. Inductively coupled plasma mass spectrometry (ICP-MS) determination of metal impurities in MWCNTs.

MWCNTs	**Ni/ppm**	**Fe/ppm**
Pristine CNTs	6.03×10^{3}	34.2
Pure CNTs	3.99×10^{3}	9.6

For pure CNT, no metal signal was detected in the surface-sensitive XPS spectra (Fig. S20a), indicating that there are no metal impurities existing on the CNT surface, while the ppm-level metal impurities detected by ICP-MS mainly come from those embedded inside the CNTs, similar with previous reports.[12] As clearly demonstrated in Ref.12, such ppm-level metal impurities ((Ni and Fe) embedded inside the CNTs avoided the contact with the electrolyte and thus make negligible contributions to the WOR activity. Furthermore, KSCN could poison metal-based active sites was added into electrolytes during WOR condition. Since no activity loss for PPDA@CNTs93 catalysts was observed, the role of the metal impurities was excluded. On the other hand, the purified CNTs shows rather inferior WOR activity (>520 mV at 10 mA cm^{-2}) in sharp contrast to that of PDDA@CNTs93 (370 mV at 10 mA cm^{-2}), implying that such trace amount of metal impurities indeed contributed little to WOR activity.

Table S3. Comparison of the performances and the relationships of selected state-of-the-art metal-free WOR catalysts in 0.1 M KOH and 1 M KOH solution.

Catalysts	**$\eta_{0.1M}$ at 10 mA cm^{-2} (mV)**	**η_{1M} at 10 mA cm^{-2} (mV)**	**$\eta_{0.1M} - \eta_{1M}$ (mV)**	**References**
PDDA@CNTs93	370	357	13	This work
N-GRW	430	360	70	Ref 20
1100-CNS	460	370	90	Ref 32
echo-MWCNTs	450	360	90	Ref 13
PEMAc@CNTs90	404	298	106	The value of η_{1M} at 10 mA cm^{-2} come from Ref 1
PAA@CNTs90	444	344	100	
PVA@CNTs90	432	356	76	
PVAc@CNTs90	457	373	84	
PEG@CNTs90	>470	390	>80	

Table S4. Comparison of the TOF value for selected state-of-art WOR electrocatalysts.

Catalysts	TOF	References
PDDA@CNTs93	0.385 s^{-1} at η = 400 mV	This work
N-GRW	0.33 s^{-1} at η = 360 mV	Ref 7a
PEMAc@CNTs90	0.38 s^{-1} at η = 300 mV	Ref 1
DR-Ni_3FeN/N-G	0.46 s^{-1} at η = 350 mV	Ref 33
Co-Ni_3N	0.0134 s^{-1} at η = 350 mV	Ref 34
Fe_1Co_1-ONS	0.022 s-1 at η = 350 mV	Ref 35
Co@NC-600	0.0126 s^{-1} at η = 420 mV	Ref 36
S-300	0.0528 s^{-1} at η = 250 mV	Ref 37

Reference

1 Y. Zhang, X. L. Fan, J. H. Jian, D. S. Yu, Z. S. Zhang and L. M. Dai, *Energy Environ. Sci*., 2017, **10**, 2312.

2 U. J. Kim, C. A. Furtado, X. M. Liu, G. G. Chen and P. C. Eklund, *J. Am. Chem. Soc*., 2005, **127**, 15437.

3 V. Datsyuk, M. Kalyva, K. Papagelis, J. Parthenios, D. Tasis, A. Siokou, I. Kallitsis and C. Galiotis, *Carbon,* 2008, **46**, 833.

4 J. Y. Cheon, J. H. Kim, J. H. Kim, K. C. Goddeti, J. Y. Park and S. H. Joo, *J. Am. Chem. Soc*., 2014, **136**, 8875.

5 G. Zhang, G. C. Wang, Y. Liu, H. J. Liu, J. H. Qu and J. H. Li, *J. Am. Chem. Soc.*, 2016, **138**, 14686.

6 M. Huynh, D. K. Bediako and D. G. Nocera, *J. Am. Chem. Soc*., 2014, **136**, 6002.

7 (a) H. B. Yang, J. W. Miao, S. F. Huang, J. Z. Chen, H. B. Tao, X. Z. Wang, L. P. Zhang, R. Chen, J. J. Gao, H. M. Chen, L. M. Dai, and B. Liu, *Sci. Adv*., 2016, **2**, e1501122. (b) J. Kibsgaard and T. F. Jaramillo, *Angew. Chem. Int. Ed*., 2014, **53**, 14433.

8 Q. Chen, L. Dai, M. Gao, S. Huang and A. Mau, *J. Phys. Chem. B.,* 2001, **105**, 618.

9 K. M. Lee, L. Li and L. Dai, *J. Am. Chem. Soc.,* 2005, **127**, 4122.

10 S. Y. Wang, D. S. Yu and L. M. Dai, *J. Am. Chem. Soc.,* 2011, **133**, 5182.

11 X. H. Chen, C. S. Chen, Q. Chen, F. Q. Cheng, G. Zhang and Z. Z. Chen, *Mater. Lett.,* 2002, **57**, 734.

12 V. Datsyuk, M. Kalyva, K. Papagelis, J. Parthenios, D. Tasis, A. Siokou, I. Kallitsis and C. Galiotis, *Carbon,* 2008, **46**, 833.

13 X. Y. Lu, W. L. Yim, B. H. R. Suryanto and C. Zhao, *J. Am. Chem. Soc.,* 2015, **137**, 2901.

14 C. C. L. McCrory, S. Jung, J. C. Peters and T. F. Jaramillo, *J. Am. Chem. Soc.,* 2013, **135**, 16977.

15 M. M. Fernández, R. M. Wagterveld, S. Ahualli, F. Liu, A. V. Delgado and H. V. M. Hamelers, *J. Power Sources,* 2016, **302**, 387.

16 Y. Lauw, M. D. Horne, T. Rodopoulos, A. Nelson and F. A. M. Leermakers, *J. Phys. Chem. B*, 2010, **114**, 11149.

17 A. G. Pandolfo and A. F. Hollenkamp, *J. Power Sources,* 2006, **157**, 11.

18 L. Wei, and G. Yushin, *Nano Energy,* 2012, **1**, 552.

19 (a) C. N. Ho and J. Hwang, *J. Electroanal. Chem*., 1994, **377**, 177. (b) J. Masa, W. Xia, I. Sinev, A. Q. Zhao, Z. Y. Sun, S. Grutzke. P. Weide, M. Muhler and W. Schuhmann, *Angew. Chem. Int. Ed,* 2014, **53**, 8508. (c) L. J. J. Janssen and E. Barendrecht, *Electrochim. Acta* 1979, **24**, 693.

20 H. B. Yang, J. W. Miao, S. F. Hung, J. Z. Chen, H. B. Tao, X. Z. Wang, L. P. Zhang, R. Chen, J. J. Gao, H. M. Chen, L. M. Dai and B. Liu, *Sci. Adv.,* 2016, **2**: e1501122.

21 (a) B. Q. Li, Z. J. Xia, B. S. Zhang, C. Tang, H. F. Wang and Q. Zhang, *Nat. Commun*. 2017, **8**, 934. (b) H. C. Li, Y. J. Zhang, X. Hu, W. J. Liu, J. J. Chen and H. Q. Yu, *Adv. Energy Mater*. 2017, 1702734. (c) T. Y. Ma, S. Dai, M. Jaroniec and S. Z. Qiao, *Angew. Chem. Int. Ed.* 2014, **53**, 7281. (d) M. Shim, A. Javey, N. W. S. Kam and H. J. Dai, *J. Am. Chem. Soc*., 2001, **123**, 11512. (e) S. Zhang, P. Kang, S. Ubnoske, M. K. Brennaman, N. Song, R. L. House, J. T. Glass and T. J. Meyer, *J. Am. Chem. Soc*. 2014, **136**, 7845.

22 H. J. Shin, S. M. Kim, S. M. Yoon, A. Benayad, K. K. Kim, S. J. Kim, H. K. Park, J. Y. Choi and Y. H. Lee, *J. Am. Chem. Soc.,* 2008, **130**, 2062.

23 H. Xu, X. Wang, Y. Zhang and S. Liu, *Chem. Mater.,* 2006, **18**, 2929.

24 Y. Liu, H. Cheng, M. Lyu, S. Fan, Q. Liu, W. Zhang, Y. Zhi, C. Wang, C. Xiao, S. Wei, B. Ye and Y. Xie, *J. Am. Chem. Soc.,* 2014, **136**, 15670.

25 G. Jiang, C. Cheng, D. Li, J. Z. Liu, *Nano Res.,* 2016, **9**, 174.

26 P. Y. Wang, M. Y. Yan, J. S. Meng, G. P. Jiang, L. B. Qu, X. L. Pan, J. Z. Liu and L. Q. Mai, *Nat. Commun*., 2017, **8**, 645.

27 Z. H. Wen, S. Q. Ci, Y. Hou and J. H. Chen, *Angew. Chem, Int. Ed.,* 2014, **53**, 6496.

28 J. Q. Tian, Q. Liu, A. M. Asiri, K. A. Alamry and X. P. Sun, *ChemSusChem*., 2014, **7**, 2125.

29 N. Y. Cheng, Q. Liu, J. Q. Tian, Y. R. Xue, A. M. Asiri, H. F. Jiang, Y. Q. He, X. P. Sun, *Chem. Commun.,* 2015, **51**, 1616.

30 Y. Zhao, R. Nakamura, K. Kamiya, S. Nakanishi, K. Hashimoto, *Nat. Commun.,* 2013, **4**, 2390.

31 G. L. Tian, M. Q. Zhao, D. S. Yu, X. Y. Kong, J. Q. Huang, Q. Zhang and F. Wei, *Small,* 2014, **10**, 2251.

32 Z. X. Pei, H. F. Li, Y. Huang, Q. Xue, Y. Huang, M. S. Zhu, Z. W. Wang and C. Y. Zhi, *Energy Environ. Sci.,* 2017, **10**, 742.

33 S. L. Zhao, M. Li, M. Han, D. D. Xu, J. Yang, Y. Lin, N. E. Shi, Y. N. Lu, R. Yang, B. T. Liu, Z. H. Dai and J. C. Bao, *Adv. Funct. Mater*., 2018, **28**, 1706018.

34 C. G. Zhu, A. L. Wang, W. Xiao, D. L. Chao, X. Zhang, N. H. Tiep, S. Chen, J. N. Kang, X. Wang, J. Ding, J. Wang, H. Zhang and H. J. Fan, *Adv. Mater.*, 2018, **30**, 1705516.

35 L. H. Zhuang, L. Ge, Y. S. Yang, M. R. Li, Y. Jia, X. D. Yao and Z. H. Zhu, *Adv. Mater.*, 2017, 29, 1606793.

36 A. Sivanantham, P. Ganesan, L. Estevez, B. P. McGrail, R. K. Motkuri and S. Shanmugam, *Adv. Energy Mater.*, 2018, 8, 1702838.

37 J. W. Su, R. X. Ge, K. M. Jiang, Y. Dong, F. Hao, Z. Q. Tian, G. X. Chen, L. Chen, *Adv. Mater.*, 2018, 1801351.